Letter

Unusual temperature dependence of thermal conductivity due to phonon resonance scattering by point defects in cubic BN

Guotai Li,[1,2] Jiongzhi Zheng,[3] Zheng Cui,[1,2] and Ruiqiang Guo[2,*]

[1]*Institute of Thermal Science and Technology, Shandong University, Jinan, Shandong 250061, China*

[2]*Thermal Science Research Center, Shandong Institute of Advanced Technology, Jinan, Shandong 250103, China*

[3]*Thayer School of Engineering, Dartmouth College, Hanover, New Hampshire 03755, USA*

(Received 5 February 2024; revised 10 July 2024; accepted 12 July 2024; published 8 August 2024)

Phonon resonance scattering caused by point defects has long been believed to be able to induce an abnormal temperature dependence of thermal conductivity κ that significantly deviates from the prediction of Rayleigh scattering. However, a rigorous demonstration and microscopic origin of this behavior are still lacking. Here, using an *ab initio* Green's function approach, we show that three types of point defects cause phonon resonance scattering in cubic BN, among which only the nitrogen vacancy indeed produces an unusual nonmonotonic temperature dependence of κ. This abnormal behavior arises only when the phonon resonance is sufficiently strong and occurs at relatively low phonon frequencies, which overwhelms the intrinsic scattering of low-frequency phonons that otherwise would produce a monotonic temperature dependence of κ. Our work provides deep insights into the phonon resonance caused by point defects and will benefit the manipulation of κ by defect engineering, particularly for doping scenarios.

DOI: 10.1103/PhysRevB.110.L060101

Point defects that are ubiquitous in solids can strongly scatter phonons and thereby largely reduce thermal conductivity κ, especially at low temperatures or at high defect concentrations. The scattering of phonons by point defects has been of fundamental interest for a century [1–6] and has been attracting increasing attention in recent years due to its important influence on heat dissipation and performance of electronics, thermoelectrics, optoelectronics, etc. [6–9]. Essentially, the phonon-defect scattering originates from the perturbation caused by the change of atomic mass and/or interatomic interactions around the defect sites, which modifies the potential energy surfaces [2]. In particular, when the perturbation is sufficiently strong, phonon resonance can rise and result in an exceptionally large suppression of κ [10,11]. Previous studies indicate that such resonance scattering occurs fortuitously, which may be induced by vacancies or substitutional atoms that introduce a slight asymmetry in the host lattice [11–14].

A unique feature induced by the phonon resonance scattering has been believed to be an abnormal temperature dependence of κ, but is without proof. The relevant studies can be traced back to 1962 [12], when phonon resonance scattering was introduced by Pohl as an additional scattering term to explain the pronounced "dip" in the κ curve versus temperature for KCl crystals containing small concentrations of KNO_2, an abnormal behavior that cannot be explained by commonly assumed Rayleigh scattering for point defects. Similar behaviors were observed subsequently by several thermal measurements for GaSb [15], KBr [16], HgSe [17], ZnS [18], etc. Also, evidence of the low-frequency resonant modes has been provided by far-infrared transmission spectra measurements [19–22] and inelastic neutron scattering [23]. However, whether the abnormal temperature dependence of κ arises from phonon resonance has not been rigorously demonstrated because of four main treatments in calculating κ:

(i) The phonon resonance scattering rates were estimated using phenomenological models derived for a simple mechanical oscillator.

(ii) The phonon resonance frequencies were predicted using an Einstein oscillator or simplified models based on force constants with limited accuracy.

(iii) Rayleigh scattering was assumed for all the other modes except for the resonance ones.

(iv) Callaway-like models considering many fitting parameters were used to calculate the κ.

Rigorous calculation of phonon-defect scattering rates is the key to identifying the effect of phonon resonance scattering on κ and the underlying mechanisms. Beyond the phenomenological models, the *ab initio* Tamura model [24], a more accurate method based on Born approximation, has later been applied to calculate the phonon-defect scattering rates. Despite its success for isotopes, this model fails to capture the phonon resonance scattering because it considers only the lowest-order perturbation [25,26]. The recently developed *ab initio* Green's function method [27,28] provides a powerful tool for accurately calculating phonon-defect scattering by treating the perturbation to all orders. This approach can well capture the behavior of the phonon resonance scattering caused by point defects [11,14,25,29]. In particular, using this approach, Katre *et al.* predict a strong phonon resonance scattering caused by broken structural symmetry for the B substitution at the C sites in SiC, which results in a much stronger suppression of κ than other defect types including the vacancies [11]. To date, this state-of-the-art Green's function

*Contact author: ruiqiang.guo@iat.cn

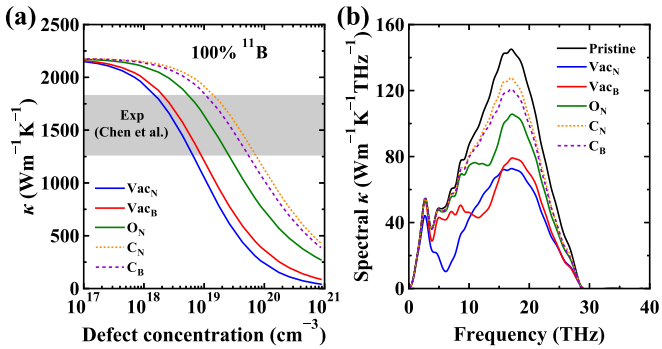

FIG. 1. Effects of point defects (Vac_N, Vac_B, O_N, C_N, and C_B) on the thermal conductivity of isotope-enriched c-BN (100% ^{11}B) at 300 K. (a) Thermal conductivity as a function of defect concentration. (b) Spectral thermal conductivity as a function of phonon frequency for 0.01% (8.7×10^{18} cm^{-3}) point defects. The gray area corresponds to the experimental results reported by Chen *et al.* [38].

approach has been used to study phonon scattering by point defects in various materials [11,14,25,26,29–36].

In this study, we have employed the *ab initio* Green's function approach to investigate the phonon resonance in cubic boron nitride (c-BN), an ultrawide-band-gap semiconductor with high κ that has attracted intense interest recently due to its potential applications in high-power electronics and optoelectronics [37,38]. We demonstrate that an abnormal nonmonotonic temperature dependence of κ indeed can be induced by phonon resonance scattering caused by point defects. This abnormal behavior arises only when the phonon resonance scattering is sufficiently strong and occurs at relatively low phonon frequencies, which overwhelms the intrinsic scattering of low-frequency phonons that otherwise would produce a monotonic temperature dependence of κ.

We obtained the phonon-defect scattering rates using our in-house Green's function code [34,36], which was used to calculate the κ of c-BN with point defects by iteratively solving the linearized Peierls-Boltzmann transport equation (PBTE) using a revised version of ShengBTE [39]. Within the framework of the Green's function method, point defects are assumed to be randomly distributed and isolated from each other. Details about the calculations are presented in the Supplemental Material [40].

Figure 1(a) shows the calculated κ of isotope-enriched c-BN (100% ^{11}B) at 300 K as a function of defect concentration for different point defects that possibly exist according to previous experimental and computational studies [38,48–51]. Specifically, the considered point defects include the intrinsic vacancies (Vac_N and Vac_B), oxygen (O_N) and carbon (C_N) substitutions at the N sites, as well as carbon (C_B) substitutions at the B sites. For comparison, we also show the κ of isotope-enriched c-BN (99.2% ^{11}B) measured by Chen *et al.* [38], as indicated by the gray area. The pristine κ calculated in the present study is 2179 W m^{-1} K^{-1}, which is relatively higher than the upper bound (1830 W m^{-1} K^{-1}) of the experimental results and agrees with the result (2145 W m^{-1} K^{-1}) predicted by Lindsay *et al.* [52]. Note that using an isotope enrichment of 99.2% ^{11}B decreases the κ to 1785 W m^{-1} K^{-1}, very close to the experimental value [38]. The lower bound of the gray area implies a defect concentration of 6×10^{18} to 7×10^{19} cm^{-3} in the samples, which falls within the range (10^{18} to 10^{20} cm^{-3}) reported by Chen *et al.* [38].

For the defect concentration $< 10^{18}$ cm^{-3}, the κ of c-BN is little reduced by point defects and approaches the magnitude of the perfect crystal. As the defect concentration increases, κ decreases substantially and largely depends on the type of point defects, indicating a scattering strength in the descending order of $Vac_N > Vac_B > O_N > C_B > C_N$. In particular, the suppression of κ by vacancies is remarkably stronger. For example, when the defect concentration increases to 8.7×10^{18} cm^{-3} (0.01%), Vac_N and Vac_B reduce κ by 48.6% and 41.6%, respectively, which are much larger than that by O_N (22.4%), C_B (13.4%), and C_N (10.6%).

We then calculated the spectral κ versus phonon frequency for c-BN with 0.01% point defects to understand the suppression of κ by defects in detail, particularly for that by vacancies. As shown in Fig. 1(b), both vacancies result in a much larger reduction of κ within the frequency range 3–27 THz than the three types of substitutions. In particular, Vac_N causes exceptionally strong suppression of κ in the frequency range 4–10 THz, as featured by the dip in the spectra.

Similarly, for the c-BN with natural isotopes (78.3% ^{11}B), Vac_N results in the largest reduction of κ among the considered point defects (see Fig. S3 in Supplemental Material [40]). Compared to the isotope-enriched case, the natural isotopes strongly reduce the κ from 2179 to 903 W m^{-1} K^{-1}, which mainly occurs within 5–28 THz. As a result, the further suppression of κ by point defects becomes much weaker after considering the natural isotope effect. Nevertheless, for the same amount (0.01%) of Vac_N, a unique dip is observed in its spectral κ around the same frequency range, further demonstrating the anomalously strong extrinsic phonon scattering.

To understand the strong suppression of κ by Vac_N, in Fig. 2(a) we plot the phonon-defect scattering rates for a defect concentration of 0.01%, in comparison with phonon-phonon and phonon-isotope scattering. A prominent peak around 6.2 THz is observed for the phonon-defect scattering rates caused by Vac_N, which are comparable to or even stronger than the phonon-phonon scattering rates at 300 K within 4–10 THz, and thus explains the unique dip observed in the spectral κ. For Vac_B, an even sharper peak is observed for its scattering rates near 4.0 THz, whose magnitude, however, is smaller than the phonon-phonon term for most modes. This is why Vac_B results in a much weaker suppression of κ, in comparison with the Vac_N case.

The peaks observed for both vacancies bear the typical signature of phonon resonance scattering [11,14,25]. This resonance behavior is further identified by the marked peaks in the imaginary part of the trace of the **T** matrix [see Fig. 2(b)], which occurs at the corresponding frequencies observed in the phonon scattering rates. One can also note a clear resonance peak for O_N at a relatively higher frequency (13.9 THz). This phonon resonance mainly accounts for the notably larger phonon scattering rates within 10–20 THz relative to those induced by C_N and C_B.

According to scattering theory, phonon resonance scattering occurs when the localized perturbation is sufficiently

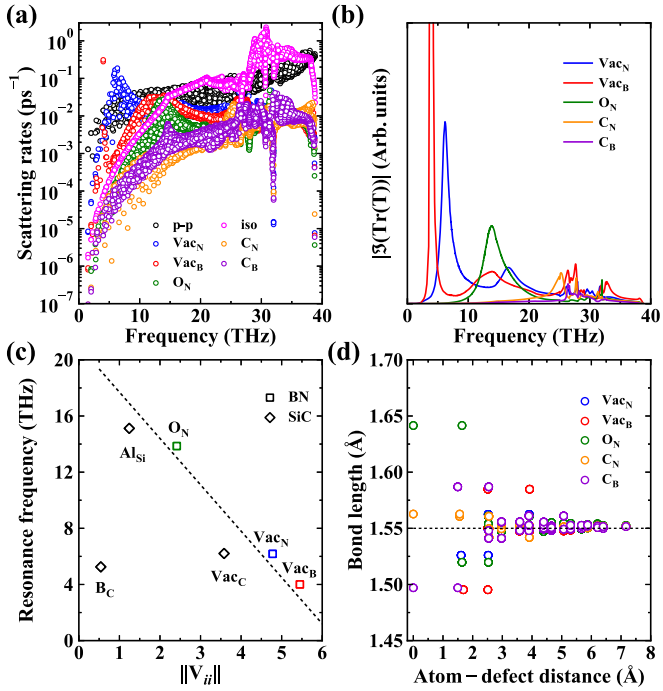

FIG. 2. (a) The phonon modal scattering rates caused by different point defects (Vac_N, Vac_B, O_N, C_N, and C_B) with a concentration of 0.01% (8.7×10^{18} cm^{-3}), in comparison with the phonon-phonon (p-p) and natural phonon-isotope (iso) scattering terms for c-BN. (b) The trace of the imaginary part of the **T** matrix as a function of frequency for each defect. (c) Resonance frequency versus the Frobenius norm of the perturbation in mass-weighted self-interaction IFCs for Vac_N, Vac_B, and O_N in c-BN, as well as Vac_C, B_C, and Al_{Si} in SiC reported by Katre *et al.* [11]. (d) Bond length as a function of the distance away from the defect site. The dashed line corresponds to the bond length (1.55 Å) of the perfect c-BN.

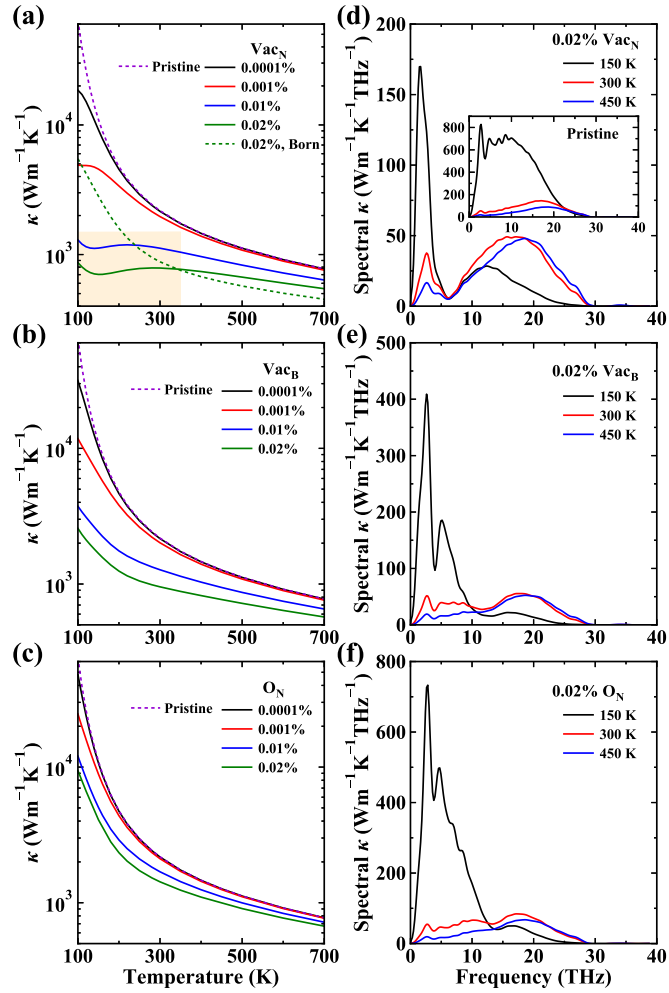

FIG. 3. The temperature dependence of the thermal conductivity for isotope-enriched c-BN with the point defects (a) Vac_N, (b) Vac_B, and (c) O_N. Four concentrations (0.0001%, 0.001%, 0.01%, and 0.02%) are considered for each point defect. The shaded region highlights the unusual nonmonotonic temperature dependence of thermal conductivity, featured by a dip between 100 and 200 K. The dashed green line is the result calculated by the Born approximation. Spectral thermal conductivity as a function of phonon frequency at varying temperatures (150, 300, and 450 K) for c-BN with 0.02% (d) Vac_N, (e) Vac_B, and (f) O_N. The inset shows the spectral thermal conductivity of the pristine c-BN.

strong. In Fig. 2(c), we show the resonance frequency as a function of the strength of local perturbation induced by point defects in c-BN, along with those in SiC [11]. We note that the resonance frequency decreases as the perturbation becomes stronger for all point defects except for B_C. This observation agrees with the expectation that a stronger localized perturbation leads to lower resonance frequency according to scattering theory [10]. It should be noted that larger perturbation does not necessarily result in stronger phonon scattering. As presented here, compared to Vac_N, Vac_B causes larger perturbation but relatively weaker phonon scattering, which can be ascribed to the smaller phonon density of states where the phonon resonance occurs.

The case of B_C in SiC is attributed to the asymmetry in the first-neighbor shell induced by the B substitution, as reported by Katre *et al.* [11]. Essentially, the asymmetry strongly modifies the curvature of the potential energy landscape near the potential minima as compared to the perfect crystal, thereby producing larger variations in the interatomic force constants (IFCs) near the point defect. To look into the structural distortion caused by the point defects in c-BN, we plot the bond length with respect to the atom-defect distance. As shown in Fig. 2(d), for all point defects, no asymmetry in the first-neighbor shell is observed, preserving the T_d symmetry. Therefore, the perturbation induced by the three substitutions is much weaker than that by vacancies. Also, the significant change in bonding length extends up to the second-nearest neighbors (2.54 Å) for all except Vac_B (relatively larger and up to 3.92 Å), indicating the perturbation is strongly localized.

We next look into how the phonon resonance affects the temperature dependence of κ in c-BN. Figures 3(a)–3(c) show the κ from 100 to 700 K for c-BN containing Vac_N, Vac_B, and O_N with varying defect concentrations, respectively. A sharp difference is observed between the results for Vac_N and other point defects. Specifically, when the defect concentration is larger than 0.001%, Vac_N induces an abnormal nonmonotonic temperature dependence in κ below 300 K, featured by a dip between 100 and 200 K, as shown in the shading in Fig. 3(a), in contrast to the commonly observed

monotonic one throughout the entire temperature range for other point defects (see the results for C_N and C_B in Fig. S4 in the Supplemental Material [40]). Also, as the defect concentration increases, the abnormal behavior caused by Vac_N occurs at a higher temperature, which is expected because the increasing phonon-defect scattering can compete with stronger phonon-phonon scattering. Note that this abnormal temperature dependence cannot be identified by Born approximation [see the dashed green line in Fig. 3(a)] based on the lowest-order perturbation theory, which fails to capture the phonon resonance scattering. When only mass difference is considered, the Born approximation is equivalent to the Tamura model that is widely used to calculate phonon-isotope scattering [24]. Meanwhile, it is noted that, for a fixed defect concentration, the temperature dependence of κ above 300 K is weakest for the Vac_N case. This is because Vac_N causes the strongest phonon-defect scattering, which becomes more dominant and results in a larger reduction in κ as temperature decreases.

To understand the abnormal temperature dependence of κ, in Figs. 3(d)–3(f), we plotted the spectral κ versus the phonon frequency for each point defect with a 0.02% concentration around the temperature where the nonmonotonic behavior occurs, namely, 150, 300, and 450 K. Specifically, the κ of c-BN with 0.02% Vac_N first increases from 705 $W\,m^{-1}\,K^{-1}$ at 450 K to 787 $W\,m^{-1}\,K^{-1}$ at 300 K, then decreases to 702 $W\,m^{-1}\,K^{-1}$ at 150 K. Essentially, the temperature dependence of κ is determined by the competition between phonon heat capacity and phonon scattering rates, both becoming larger as temperature increases (see Figs. S5 and S6 in the Supplemental Material [40]). Specifically, the temperature dependence of κ is dominated by heat capacity at low temperatures (well below the Debye temperature) and phonon-phonon scattering at high temperatures (above the Debye temperature). As shown in the inset of Fig. 3(d), the spectral κ of the perfect c-BN crystal decreases throughout almost the entire frequency range up to 28 THz as temperature increases from 150 to 450 K, indicating the dominance of phonon scattering rates throughout the entire frequency range. After point defects are introduced, phonon-defect scattering suppresses the spectral κ of all frequencies and changes its temperature dependence within the high-frequency range of ~12 to 28 THz for each type of point defect, indicating the dominance of heat capacity at the high-frequency range. For example, we show how the competition between heat capacity and lifetime affects the temperature dependence of κ contributed by two specific phonon modes [named as mode #1 with a relatively low frequency of 4.95 THz at $\mathbf{q} = (0.13, 0.06, 0.03)$ and mode #2 with a much higher frequency of 19.71 THz at $\mathbf{q} = (0.29, 0.06, 0.03)$] in Fig. S7 in the Supplemental Material [40]. For mode #1, heat capacity dominates the increase in κ from 150 to 200 K while phonon lifetime leads to a decrease in κ from 200 to 450 K. For mode #2, heat capacity dominates κ over almost the entire temperature range 150–450 K. The major difference is the Vac_N results in substantially larger suppression of κ than Vac_B and O_N below 12 THz, particularly around the resonance frequency 6.2 THz induced by Vac_N. For the Vac_N case, the strong phonon resonance scattering reduces its κ contribution below 12 THz to be comparable to that above at 150 K, thereby resulting

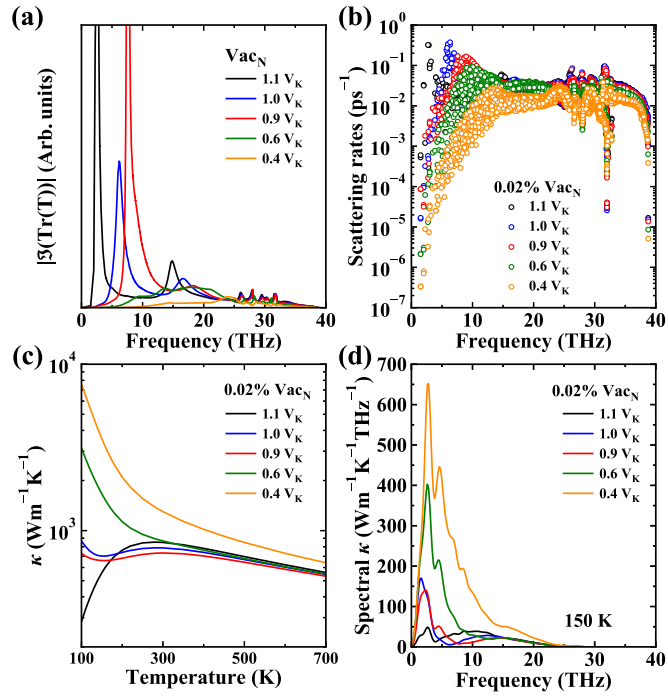

FIG. 4. Effect of the IFC perturbation strength caused by Vac_N on (a) the trace of the imaginary part of the **T** matrix, (b) phonon-defect scattering rates, (c) thermal conductivity, and (d) spectral thermal conductivity as a function of phonon frequency at 150 K. A defect concentration of 0.02% is considered for all cases.

in a lower overall κ at 150 K than at 300 K. In contrast, although the phonon resonance induced by Vac_B occurs at even lower frequencies, its strength is not large enough to suppress the dominance of low-frequency phonons in determining the overall temperature dependence of κ. As for the O_N case, because the phonon resonance scattering occurs at much higher frequencies, it cannot change the temperature dependence of κ, no matter how strong the resonance is.

As presented above, the abnormal temperature dependence of κ arises only when the phonon resonance scattering is strong enough and occurs at relatively low phonon frequencies. To further verify this, we have artificially modified the perturbation strength induced by Vac_N and investigated its influence on the phonon resonance behavior and thermal conductivity. As shown in Fig. 4(a), the trace of the imaginary part of the **T** matrix indicates that the phonon resonance scattering occurs for stronger perturbations ($0.9\mathbf{V}_K$, $1.0\mathbf{V}_K$, and $1.1\mathbf{V}_K$) but disappears for relatively smaller perturbation ($0.4\mathbf{V}_K$ and $0.6\mathbf{V}_K$). Meanwhile, the resonant frequency decreases from 7.5 to 2.7 THz as the perturbation strength increases from $0.9\mathbf{V}_K$ to $1.1\mathbf{V}_K$, agreeing with the trend shown in Fig. 2(c). These observations further demonstrate that large perturbation is required to induce phonon resonance and stronger perturbation results in a lower resonant frequency.

The phonon resonance strongly modifies the strength of phonon-defect scattering. As shown in Fig. 4(b), the phonon-defect scattering rates exhibit prominent peaks around the resonant frequency and substantially decrease as the perturbation strength decreases. Figure 4(c) further shows the temperature-dependent κ for 0.02% Vac_N with varying IFC perturbation. As expected, the phonon resonance scattering

results in a nonmonotonic temperature dependence of κ, in contrast to the monotonic one when the resonance is absent. Similarly, the spectral κ of low-frequency phonons is strongly suppressed for the resonant cases, allowing the dominance of high-frequency phonons in determining the temperature dependence of κ (see Fig. S8 in the Supplemental Material [40]). Particularly among the three resonant cases, the $1.1\mathbf{V}_K$ more strongly suppresses the κ below 170 K than $1.0\mathbf{V}_K$ and $0.9\mathbf{V}_K$, which is due to the larger reduction of spectral κ around the resonant frequency 2.7 THz [Fig. 4(d)].

In summary, we have investigated the effect of point defects on phonon scattering and κ in c-BN by combining an *ab initio* Green's function approach and the PBTE. Among the five types of point defects considered in this study, Vac_N is found to result in the largest suppression of κ, which is ascribed to the strongest phonon resonance scattering within 4–10 THz induced by the localized perturbation of IFCs. Particularly when the defect concentration is larger than 0.001%, Vac_N induces an unusual nonmonotonic temperature dependence of κ below 300 K. In contrast, a monotonic one is observed for other point defects, although two of them also cause phonon resonance scattering. This is because the abnormal temperature dependence of κ arises only when the phonon resonance is strong enough and occurs at relatively low phonon frequencies, which largely suppresses the κ contribution of low-frequency phonons that otherwise would produce a monotonic temperature dependence of κ.

Our work provides a microscopic picture for the phonon resonance scattering caused by point defects and its influence on κ, which can explain the puzzle of the unusual temperature dependence of κ observed in experiments and will be helpful for manipulating thermal properties by defect engineering. In particular, the exceptionally large variation of κ by phonon resonance scattering needs to be paid special attention in the dopant selection and concentration control of semiconductor design.

We acknowledge support from the Excellent Young Scientists Fund (Overseas) of Shandong Province (Grant No. 2022HWYQ-091), the Taishan Scholars Program of Shandong Province, the Natural Science Foundation of Shandong Province (Grant No. ZR2022MA011), and the Initiative Research Fund of Shandong Institute of Advanced Technology. This work used the computational resources at Shandong Institute of Advanced Technology.

[1] R. Peierls, Zur kinetischen theorie der wärmeleitung in kristallen, Ann. Phys. **395**, 1055 (1929).
[2] P. G. Klemens, The scattering of low-frequency lattice waves by static imperfections, Proc. Phys. Soc. A **68**, 1113 (1955).
[3] J. M. Ziman, *Electrons and Phonons: The Theory of Transport Phenomena in Solids* (Clarendon Press, Oxford, UK, 1960).
[4] C. T. Walker and R. O. Pohl, Phonon scattering by point defects, Phys. Rev. **131**, 1433 (1963).
[5] L. Lindsay, C. Hua, X. L. Ruan, and S. Lee, Survey of *ab initio* phonon thermal transport, Mater. Today Phys. **7**, 106 (2018).
[6] X. Qian, J. Zhou, and G. Chen, Phonon-engineered extreme thermal conductivity materials, Nat. Mater. **20**, 1188 (2021).
[7] D. G. Cahill, P. V. Braun, G. Chen, D. R. Clarke, S. Fan, K. E. Goodson, P. Keblinski, W. P. King, G. D. Mahan, A. Majumdar, H. J. Maris, S. R. Phillpot, E. Pop, and L. Shi, Nanoscale thermal transport. II. 2003–2012, Appl. Phys. Rev. **1**, 011305 (2014).
[8] Y. Zheng, T. J. Slade, L. Hu, X. Y. Tan, Y. Luo, Z. Z. Luo, J. Xu, Q. Yan, and M. G. Kanatzidis, Defect engineering in thermoelectric materials: What have we learned? Chem. Soc. Rev. **50**, 9022 (2021).
[9] R. Hanus, R. Gurunathan, L. Lindsay, M. T. Agne, J. Shi, S. Graham, and G. Jeffrey Snyder, Thermal transport in defective and disordered materials, Appl. Phys. Rev. **8**, 031311 (2021).
[10] E. Economou, *Green's Functions in Quantum Physics* (Springer, New York, 1983), pp. 108–109.
[11] A. Katre, J. Carrete, B. Dongre, G. K. H. Madsen, and N. Mingo, Exceptionally strong phonon scattering by B substitution in cubic SiC, Phys. Rev. Lett. **119**, 075902 (2017).
[12] R. O. Pohl, Thermal conductivity and phonon resonance scattering, Phys. Rev. Lett. **8**, 481 (1962).
[13] J. W. Schwartz and C. T. Walker, Phonon scattering by lattice vacancies, Phys. Rev. Lett. **16**, 97 (1966).
[14] B. Dongre, J. Carrete, A. Katre, N. Mingo, and G. K. H. Madsen, Resonant phonon scattering in semiconductors, J. Mater. Chem. C **6**, 4691 (2018).
[15] M. G. Holland, Phonon scattering in semiconductors from thermal conductivity studies, Phys. Rev. **134**, A471 (1964).
[16] F. C. Baumann, J. P. Harrison, R. O. Pohl, and W. D. Seward, Thermal conductivity in mixed alkali halides: KCl:Li and KBr:Li, Phys. Rev. **159**, 691 (1967).
[17] D. A. Nelson, J. G. Broerman, E. C. Paxhia, and C. R. Whitsett, Resonant phonon scattering in mercury selenide, Phys. Rev. Lett. **22**, 884 (1969).
[18] G. A. Slack, Thermal conductivity of II-VI compounds and phonon scattering by Fe^{2+} impurities, Phys. Rev. B **6**, 3791 (1972).
[19] A. J. Sievers and S. Takeno, Isotope shift of a low-lying lattice resonant mode, Phys. Rev. **140**, A1030 (1965).
[20] S. Takeno and A. J. Sievers, Characteristic temperature dependence for low-lying lattice resonant modes, Phys. Rev. Lett. **15**, 1020 (1965).
[21] R. D. Kirby, I. G. Nolt, R. W. Alexander, and A. J. Sievers, Far infrared properties of lattice resonant modes. I. Isotope shifts, Phys. Rev. **168**, 1057 (1968).
[22] A. M. Kahan, M. Patterson, and A. J. Sievers, Far-infrared properties of lattice resonant modes. VI. Hydrostatic pressure effects, Phys. Rev. B **14**, 5422 (1976).
[23] H. B. Møller and A. R. Mackintosh, Observation of resonant lattice modes by inelastic neutron scattering, Phys. Rev. Lett. **15**, 623 (1965).
[24] S. I. Tamura, Isotope scattering of dispersive phonons in Ge, Phys. Rev. B **27**, 858 (1983).
[25] N. A. Katcho, J. Carrete, W. Li, and N. Mingo, Effect of nitrogen and vacancy defects on the thermal conductivity of

diamond: An *ab initio* Green's function approach, Phys. Rev. B **90**, 094117 (2014).

[26] N. H. Protik, J. Carrete, N. A. Katcho, N. Mingo, and D. Broido, *Ab initio* study of the effect of vacancies on the thermal conductivity of boron arsenide, Phys. Rev. B **94**, 045207 (2016).

[27] N. Mingo, K. Esfarjani, D. A. Broido, and D. A. Stewart, Cluster scattering effects on phonon conduction in graphene, Phys. Rev. B **81**, 045408 (2010).

[28] A. Kundu, N. Mingo, D. A. Broido, and D. A. Stewart, Role of light and heavy embedded nanoparticles on the thermal conductivity of SiGe alloys, Phys. Rev. B **84**, 125426 (2011).

[29] A. Kundu, F. Otte, J. Carrete, P. Erhart, W. Li, N. Mingo, and G. K. H. Madsen, Effect of local chemistry and structure on thermal transport in doped GaAs, Phys. Rev. Mater. **3**, 094602 (2019).

[30] A. Katre, J. Carrete, T. Wang, G. K. H. Madsen, and N. Mingo, Phonon transport unveils the prevalent point defects in GaN, Phys. Rev. Mater. **2**, 050602(R) (2018).

[31] C. A. Polanco and L. Lindsay, *Ab initio* phonon point defect scattering and thermal transport in graphene, Phys. Rev. B **97**, 014303 (2018).

[32] C. A. Polanco and L. Lindsay, Thermal conductivity of InN with point defects from first principles, Phys. Rev. B **98**, 014306 (2018).

[33] R. Stern, T. Wang, J. Carrete, N. Mingo, and G. K. H. Madsen, Influence of point defects on the thermal conductivity in FeSi, Phys. Rev. B **97**, 195201 (2018).

[34] R. Guo and S. Lee, Mie scattering of phonons by point defects in IV-VI semiconductors PbTe and GeTe, Mater. Today Phys. **12**, 100177 (2020).

[35] C. A. Polanco, T. Pandey, T. Berlijn, and L. Lindsay, Defect-limited thermal conductivity in MoS_2, Phys. Rev. Mater. **4**, 014004 (2020).

[36] G. Li, Q. Wang, Z. Cui, and R. Guo, Competition between intrinsic and extrinsic phonon scatterings in cubic BP and BAs with point defects, Phys. Rev. B **107**, 184118 (2023).

[37] K. Watanabe, T. Taniguchi, and H. Kanda, Ultraviolet luminescence spectra of boron nitride single crystals grown under high pressure and high temperature, Phys. Status Solidi **201**, 2561 (2004).

[38] K. Chen, B. Song, N. K. Ravichandran, Q. Zheng, X. Chen, H. Lee, H. Sun, S. Li, G. A. G. Udalamatta Gamage, F. Tian, Z. Ding, Q. Song, A. Rai, H. Wu, P. Koirala, A. J. Schmidt, K. Watanabe, B. Lv, Z. Ren, L. Shi, D. G. Cahill, T. Taniguchi, D. Broido, and G. Chen, Ultrahigh thermal conductivity in isotope-enriched cubic boron nitride, Science **367**, 555 (2020).

[39] W. Li, J. Carrete, N. A. Katcho, and N. Mingo, ShengBTE: A solver of the Boltzmann transport equation for phonons, Comput. Phys. Commun. **185**, 1747 (2014).

[40] See Supplemental Material at http://link.aps.org/supplemental/10.1103/PhysRevB.110.L060101 for computational method, comparison of calculated and measured phonon dispersion, convergence of the thermal conductivity in pure c-BN with respect to the size of **q**-point mesh, effects of point defects on the thermal conductivity and spectral thermal conductivity in natural c-BN, temperature-dependent thermal conductivity and spectral thermal conductivity for isotope-enriched c-BN with C_N and C_B, heat capacity of c-BN as a function of temperature, phonon modal scattering rates caused by different point defects, competition of heat capacity and phonon lifetime, and spectral thermal conductivity at 150, 300, and 450 K for varying strength of IFC perturbations caused by Vac_N (see also Refs. [41–47] therein).

[41] M. Omini and A. Sparavigna, An iterative approach to the phonon Boltzmann equation in the theory of thermal conductivity, Physica B: Condens. Matter **212**, 101 (1995).

[42] M. Omini and A. Sparavigna, Beyond the isotropic-model approximation in the theory of thermal conductivity, Phys. Rev. B **53**, 9064 (1996).

[43] G. Kresse and J. Furthmuller, Efficient iterative schemes for *ab initio* total-energy calculations using a plane-wave basis set, Phys. Rev. B **54**, 11169 (1996).

[44] P. E. Blöchl, Projector augmented-wave method, Phys. Rev. B **50**, 17953 (1994).

[45] J. P. Perdew and A. Zunger, Self-interaction correction to density-functional approximations for many-electron systems, Phys. Rev. B **23**, 5048 (1981).

[46] A. Togo, F. Oba, and I. Tanaka, First-principles calculations of the ferroelastic transition between rutile-type and $CaCl_2$-type SiO_2 at high pressures, Phys. Rev. B **78**, 134106 (2008).

[47] J. Kikkawa, T. Taniguchi, and K. Kimoto, Nanometric phonon spectroscopy for diamond and cubic boron nitride, Phys. Rev. B **104**, L201402 (2021).

[48] T. Taniguchi and K. Watanabe, Synthesis of high-purity boron nitride single crystals under high pressure by using Ba–BN solvent, J. Cryst. Growth **303**, 525 (2007).

[49] T. Taniguchi and S. Yamaoka, Spontaneous nucleation of cubic boron nitride single crystal by temperature gradient method under high pressure, J. Cryst. Growth **222**, 549 (2001).

[50] W. Orellana and H. Chacham, Atomic geometry and energetics of vacancies and antisites in cubic boron nitride, Appl. Phys. Lett. **74**, 2984 (1999).

[51] W. Orellana and H. Chacham, Energetics of carbon and oxygen impurities and their interaction with vacancies in cubic boron nitride, Phys. Rev. B **62**, 10135 (2000).

[52] L. Lindsay, D. A. Broido, and T. L. Reinecke, First-principles determination of ultrahigh thermal conductivity of boron arsenide: A competitor for diamond? Phys. Rev. Lett. **111**, 025901 (2013).